NANOCRYSTALLINE SYSTEMS FOR PROTECTION, DETECTION AND DEMILITARIZATION

Final Report

by

Michael Grätzel, Ph.D.
Professor of Chemistry

December 19, 1995

United States Army

European Research Office of the U.S. Army
Chemistry Branch

CONTRACT NO. N68171-94-C-9148

Michael Grätzel, Ph.D.
Professor of Chemistry
Institut de Chimie Physique II
Ecole Polytechnique Fédérale
CH-1015 Lausanne, Switzerland

"The Research reported in this document has been made possible through the support and sponsorship of the US Government through its European Research Office. ~~This report is intended only for the internal management use of the Contractor and the US Government~~."

Research over the last year on grant no R & D 7504-CH-01 from the European Research Office of the U.S. Army has consisted both in the investigation of the photocatalytic activity of mammalian ferritin and in the studies of nanocrystalline oxide films, specifically WO_3 and TiO_2.

The first phase of the project concerns photocatalytic studies on small iron oxide clusters in view of the use of such iron oxide based catalysts in the demineralization of non-stockpile agents. We have initiated work on ferritin which is a very interesting natural protein, carrying in its cavity iron oxide particles with a size of approximately 5 nm. We have discovered that these quantum sized iron oxide particles have a very high activity in promoting the oxidation of a whole series of organics by oxygen, a reaction which is strongly catalysed by the band gap excitation of the semiconductor colloid.

Ferritin, an ubiquitous biological iron-storage protein molecule, consists of 24 symmetrically related protein subunits forming a near-spherical hollow shell, "apoferritin". The central cavity of the apoferritin shell is occupied by an iron core of "ferrihydrite" or $5Fe_2O_3 \cdot 9H_2O$ varying in "crystallite" structure (amorphous or crystalline) depending on the source of the ferritin which is widely distributed in nature (e.g., mammalian spleen, liver, heart or bacterial, plant or fungal ferritin.) Through our experimentation it has been shown not only that the iron (III) core can be photochemically reduced (Fe (II)) in presence of electron donors, but likewise that organic substrates such as oxalate and tartrate can be photo-oxidized, the ferrihydrite core acting as a catalyst, with the concomitant reduction of O_2. Laser photolysis studies confirmed the reduction of cytochrome C and viologens photosensitized by ferritin via band-gap excitation. (see schemes 1, 2, 3 of Fig. 1).

A schematic representation of the horse spleen ferritin molecule is shown in Fig. 2 a). The source of ferritin used in our experiments was generally Sigma type 1 from horse spleen, in sterile filtered solution in 0.1 M NaCl with a Cd content of less than 1%, although some experimentation using a Fluka source (Biochemika, 50 mg/ml aqueous solution with less than 0.05% Cd, exhibiting less activity) was performed. This lower activity was attributed to a difference in iron core structure or crystallinity. Generally, the ferritin was used as received with no prior treatment in the presence of various chelating agents, such as EDTA. Illumination was carried out employing either a Xenon lamp or in a Hanau suntest apparatus with appropriate filters. Laser photolysis was performed using a doubled frequency ruby laser.

The photoreduction of ferritin (0.25 mg/ml) in presence of 2 mM oxalate, pH 5.5 (50 mM MES buffer) under an argon atmosphere with wavelengths greater than 300 nm is presented in Fig. 3 where after 30 min. illumination practically all of the ferrihydrite is reduced to Fe(II). Re-addition of air results in immediate re-oxidation of Fe(II) to Fe(III). Fig. 4 illustrates the effect of oxalate on this photoreduction. In the absence of oxalate only a very slight reduction of ferritin is witnessed due to electron donation by the protein shell molecules. The effect of pH on this photoreduction reaction, that is, the more

acid the solution, the more rapid the reaction, is demonstrated in Fig. 5. Kinetics of the photoreduction of ferritin in presence of various electron donors such as tartrate, cysteine and ascorbate, as well as the blank (donor electrons from protein shell) are shown in Fig. 6.

The photo-oxidation and resultant full destruction of the organic compounds oxalate and tartrate with concomitant CO_2 evolution and O_2 consumption in presence of mammalian ferritin at an initial pH of 3 under suntest lamp conditions was observed. The pH in the unbuffered experiments on oxalic acid varies between 3 and 7 during the course of this reaction.

$$C_2O_4H_2 + 0.5O_2 \longrightarrow 2CO_2 + H_2O \qquad (1)$$

The photo-oxidative degradation of tartaric acid in presence of ferritin proceeds by the following overall stoichiometry

$$C_4H_4O_6 + 2O_2 \longrightarrow 4CO_2 + 2H_2O \qquad (2)$$

with the pH varying from the initial value of 3 to pH = 5.8. One could easily imagine the extension of this type of photo-oxidative degradation to various organic CW simulants, such as the organic phosphate containing pesticides.

The direct photo-electron charge transfer from photosensitized ferritin to the molecules cytochrome C and various viologens was demonstrated in laser flash photolysis experiments. These molecules are too large to enter the protein core of the ferritin molecule through one of the channels found in the shell structure and, thus, electron transfer must occur via tunneling to the exterior of the protein molecule. Fig. 2 b) and c) are schematic representations of these photoreductions. Fig. 7 illustrates the absorbance changes as a function of time both under dark and illuminated conditions. Figs. 8 and 9 depict the photoreduction of cytochrome C by ferritin with and without the presence of additional electron donors, or air, and as a function of light intensity. The reaction is greatly enhanced in the presence of tartrate. The more acid pH ranges are optimal for cytochrome C photoreduction as for photoreduction of ferritin itself in presence of oxalate;however, the reaction extent for photoreduction of cytochrome C in presence of tartrate remains unchanged over the pH range 5.5 to 8.5. The photoreduction of dimer viologen (DV) by ferritin in presence of tartrate is shown as well in Fig. 10. A flash photolysis experiment demonstrating the direct electron transfer from ferritin to PVS (propyl viologen sulfonate) in presence of tartrate as well as its blank are depicted in Fig. 11.

We have also engaged studies on nanocrystalline oxide films, as mentioned previously. The goal here is to obtain films that exhibit high photocatalytic activity under visible light. To this end, nanocrystalline WO_3 films in the micron thickness range and with a roughness factor exceeding 1000 have been produced via a colloidal precursor solution. These films have been subjected to

photoelectrochemical studies using methanol as model substrate for oxidation. Valence band hole transfer to this scavenger leading to complete mineralization was witnessed. For comparison, photoelectrochemical phenol oxidation on sensitizer-derivatized thin film TiO_2 optically transparent electrodes was also investigated.

The colloidal WO_3 precursor solution was prepared by first dissolving 3.6 gm of H_2WO_3 (tungstic acid) in 50 ml of water to which were added 4 ml of concentrated NH_3. This solution was then diluted to 800 ml and boiled for 6 hours. The final solution, a transparent colloidal solution of white tungstic acid, attains pH=3.7.

The WO_3 particulate films are prepared by adding 0.1 ml of 4% PVA (polyvinyl alcohol) to 0.1 ml of the 2 M WO_3 precursor colloidal solution and diluted to 0.24 ml by adding 0.04 ml H_2O. We then applied 0.1 ml of this mixture to a conducting glass {Nippon Sheet Glass, 10 ohm/□, fluorine-doped SnO_2 glass (TCO)} surface of 3.7 cm^2 (E 12 electrode) The film was initially dried in a stream of hot air for 5 to 10 minutes at approximately 90 °C and then sintered at 500 °C under a stream of O_2 for 1 hour. The scanning electron microscope images depicted in Fig. 12 illustrate the particulate nature of the porous film (7μ) electrode, specifically E 12, for which the preparation is described above. The white light photocurrent/voltage plots of aqueous and 1.5 M methanol solutions, respectively, employing the E 12, WO_3 working electrode are illustrated in Figs. 13 and 14, the respective bias necessary to obtain charge separation for the efficient oxidation of H_2O and methanol being demonstrated.

Fig. 15 shows the WO_3 particulate film action spectrum at pH = 3 in the photoelectrochemical oxidation of methanol (1.5 M) in aqueous solution (supporting electrolyte 0.1 M $NaClO_4$). The WE potential is adjusted to 500 mV vs SSCE. The incident monochromatic photon to current conversion yield (IPCE) is plotted as a function of excitation wavelength. The IPCE values were derived from the photocurrents (mA/cm^2) by means of the equation

$$IPCE = 1240 \cdot i_{ph}/\lambda(nm) \cdot P$$

where P is the incident monochromatic light intensity expressed in W/m^2. The ICPE values increase towards the blue steeply starting from a threshold wavelength at 480 nm. The conversion yield at 400 nm (E12 electrode) attains a value close to 75% in the absence of methanol (Fig. 16) and 115% in the presence of methanol (Fig. 15) indicating that quantitative conversion of incident photons into electric current is taking place. The fact that the yield exceeds 100% is due to the current doubling effect observed with methanol: Hole capture by the latter reagent produces a radical which injects an electron in the conduction band of WO_3. From this finding one infers that light induced charge separation is greatly favored in the nanocrystalline oxide films. The decline in efficiency at wavelengths shorter than 400 nm is an artifact due to the glass absorption as can be seen from the inset showing the absorption

spectrum of the film coated WO_3 electrode. Under polychromatic exposure the experimental photocurrent in presence of methanol was measured as 3.1 mA/cm^2, in good agreement with the value calculated of 3.8 mA/cm2 from the overlap of the photocurrent action spectrum in Fig. 15 with the standard solar AM 1.5 emission spectrum (see Table 1). In the action spectrum of the WO_3 electrode we would like to stress the long visible wavelength tail which is not apparent in the action spectrum of the photoelectrochemical oxidation by nanocrystalline TiO_2. Fig. 17 illustrates the photocurrent action spectrum of phenol oxidation using a sensitized TiO_2 particulate film as the WE for comparison with the WO_3 action spectrum of methanol oxidation. In this case the electrode is a particulate film of TiO_2 derivatized by the ruthenium complex {Ru(4,4'-2,.2'-bipy)(4'-PO_3H-terpy)(NCS)}, where (4'-PO_3H-terpy) is the novel ligand 2,2':6',2"-terpyridine-4'-phosphonic acid. The supporting electrolyte in this experiment is 0.01 M $NaClO_4$. The second curve depicted is the previous RuL_3 (ruthenium (2,2')-bipyridyl-(4,4')-dicarboxylic acid) derivatized TiO_2 film shown for comparison. The phosphonate group of this ligand stongly enhances adsorption onto the TiO_2 surface and provides sufficient electronic coupling with the oxide to achieve efficient light-induced charge separation. These experiments were carried out in an electrochemical cell equipped with a quartz window, irradiated from the glass side. The source of irradiation was a Xe lamp, 100 W/m^2 simulated sunlight with a 470 nm cut-off filter. Under these conditions any photocurrent is solely attributed to sensitisation. The photocurrent action spectrum indicates a maximum incident photon flux to electron flow conversion efficiency of 18%, compared to 13% for the RuL_3 sensitized film, at 480 nm. The photocurrent calculated for the overlap integral of the action spectra with the AM 1.5 solar emission corresponds to 1.51 mA/cm^2 for the phosphonated complex and 0.77 mA/cm^2 for the carboxylated complex, respectively. Thus the new sensitizer based on a phosphonated bipyridyl ligand exhibits a greatly improved visible light response apart from being more strongly adsorbed to TiO_2 films as compared to the previously employed RuL_3 dye.

Studies on the reproducibility and efficiency of these nanocrystalline WO_3 thin film electrodes have advanced greatly. Visible light photoelectrochemical degradation of the simulant compound, 4-nitrophenyldiethylphosphate, Paraoxon, is proving to be quite promising, and will be addressed in a forthcoming report.

Photoreduction of Ferritin in the Presence of Electron Donors

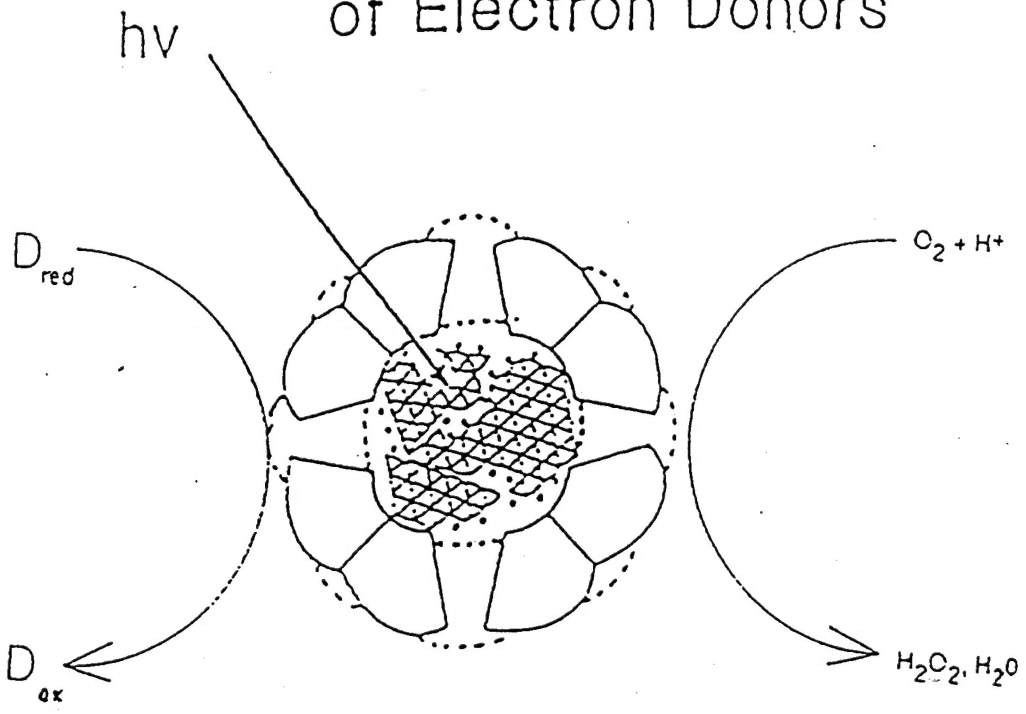

FIGURE 1

The Photochemical Activity of Mammalian Ferritin

1)

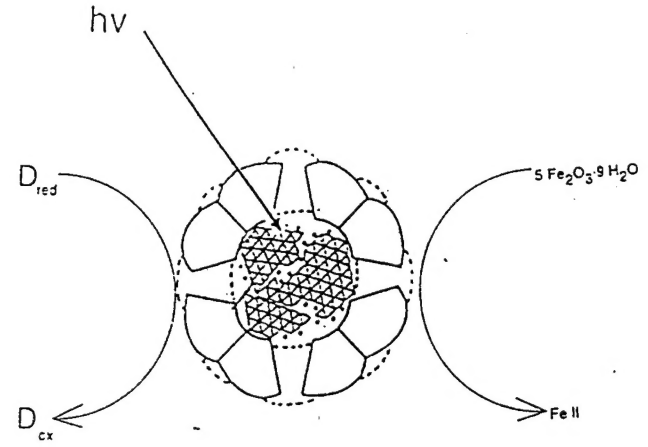

Photoreduction of Ferritin in the Presence of Electron Donors

2)

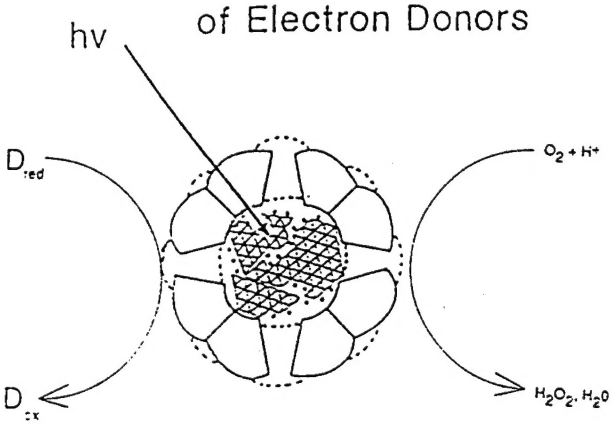

Photooxidation of the Organic Substrates in the Presence of Ferritin

3)

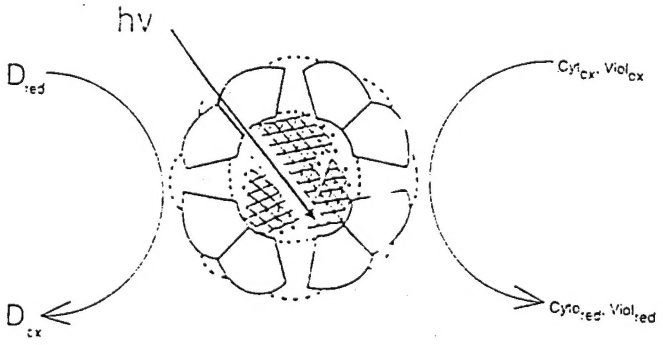

Reduction of Cytochrome c and Viologenes photosensitized by Ferritin

FIGURE 2

Schematic representation of the horse spleen ferritin molecule

a

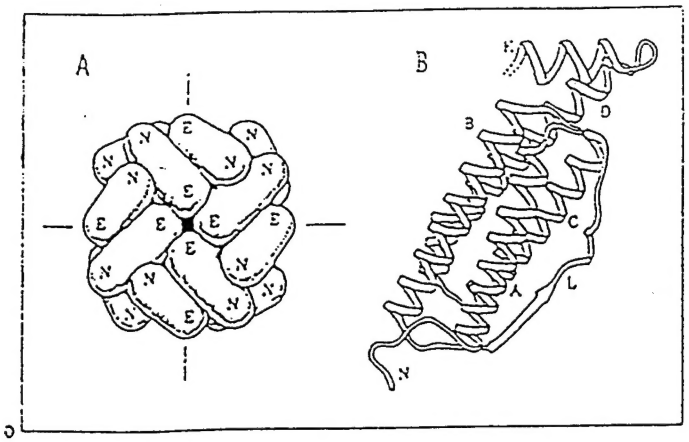

b

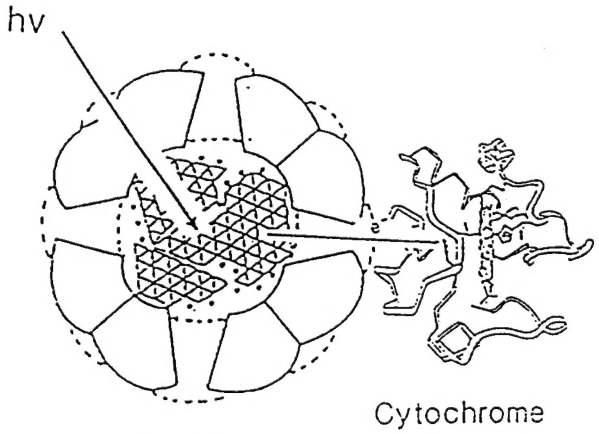

c

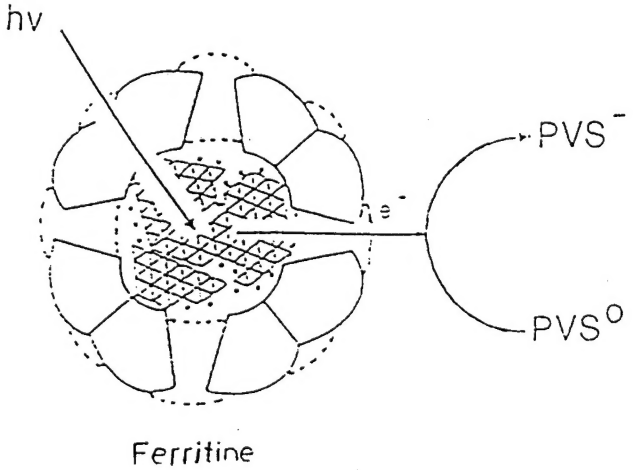

FIGURE 3

Photoreduction of Ferritin in the Presence of Oxalate

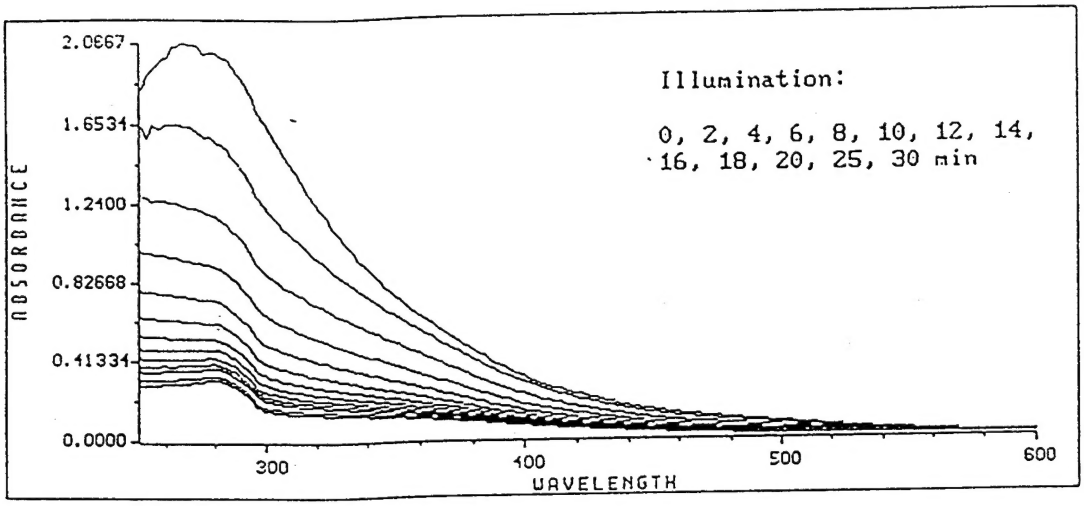

oxalate, 0.018M, pH 5.0, L>300 nm

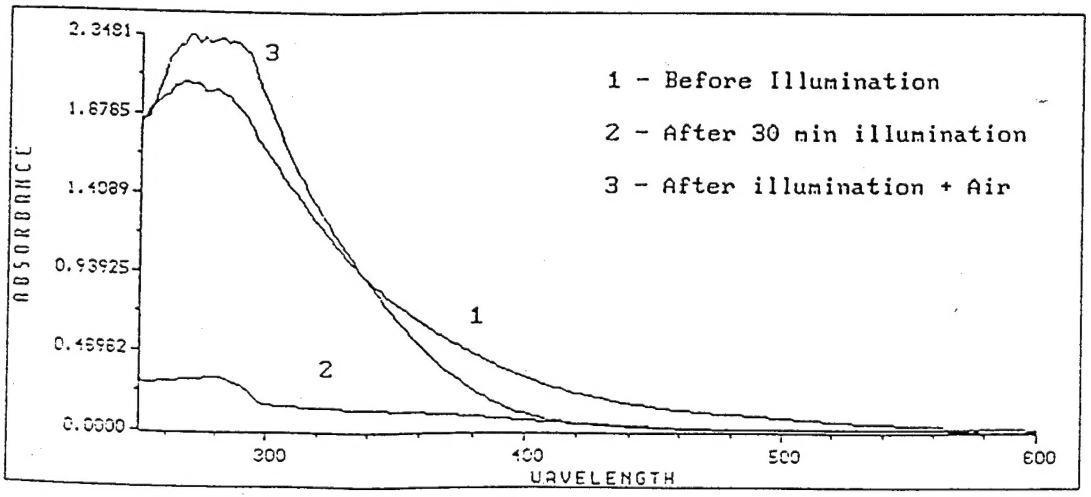

FIGURE 4

Photoreduction of Ferritin in the Presence of Oxalate. Kinetics.

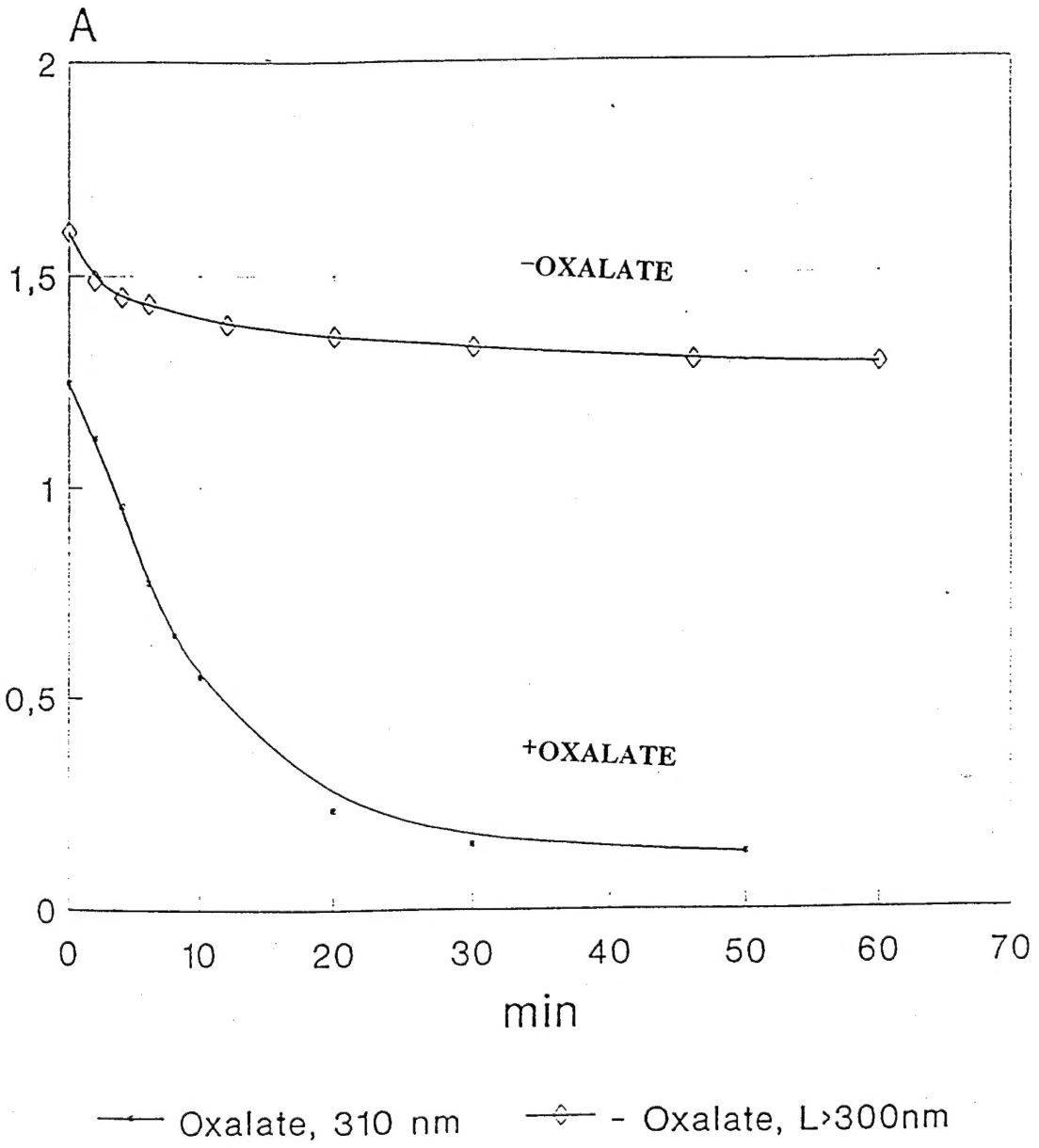

0.25mg/ml Ferritin, 20mM Oxalate,
pH 5.5, 50 mM MES, Light>300nm,>460nm

FIGURE 5

Photoreduction of Ferritin in the Presence of Oxalate as a Function of pH

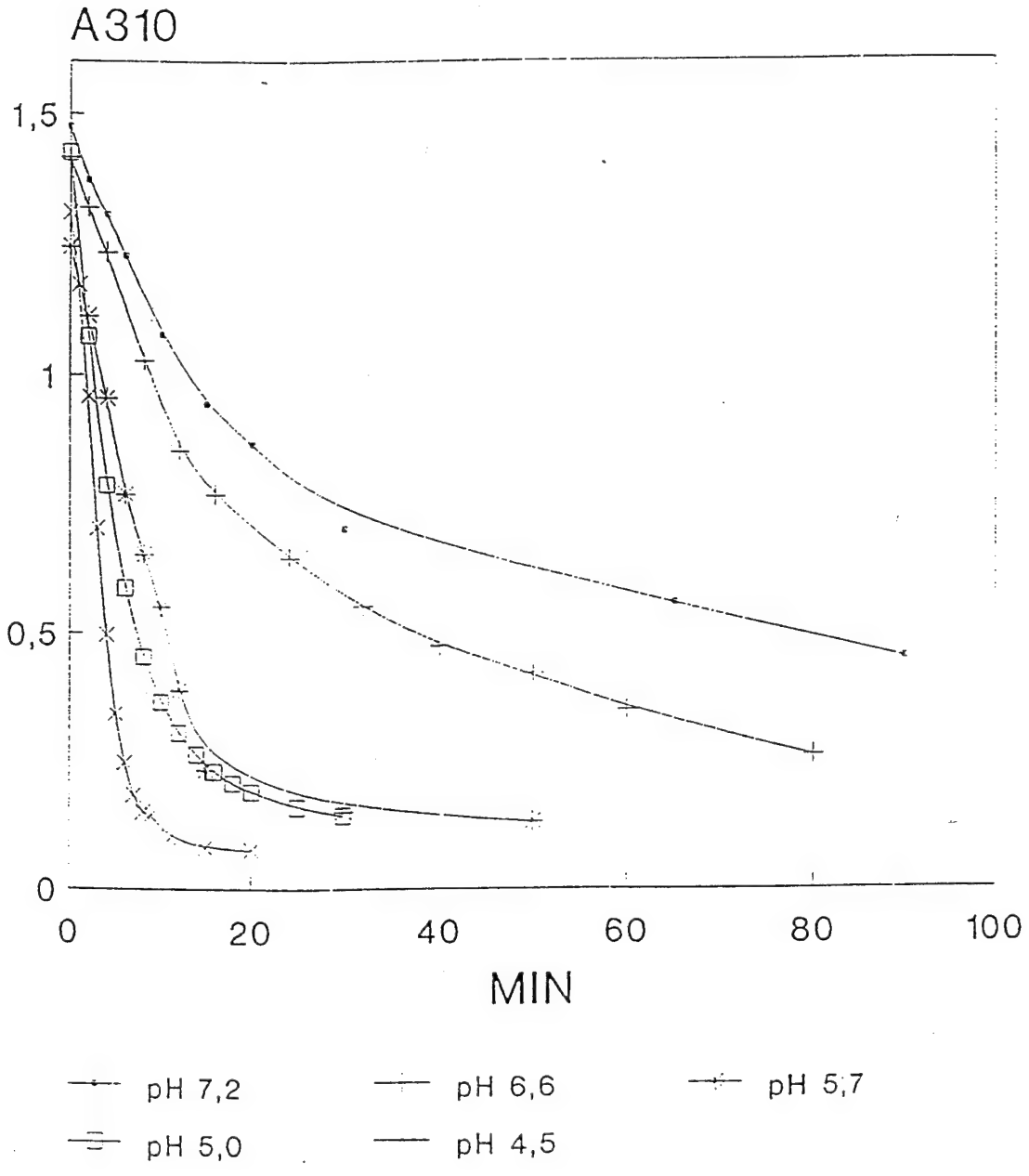

Oxalate 20mM, Fer 0,5mkM; L>300nm

FIGURE 6

Photoreduction of Ferritin Kinetics

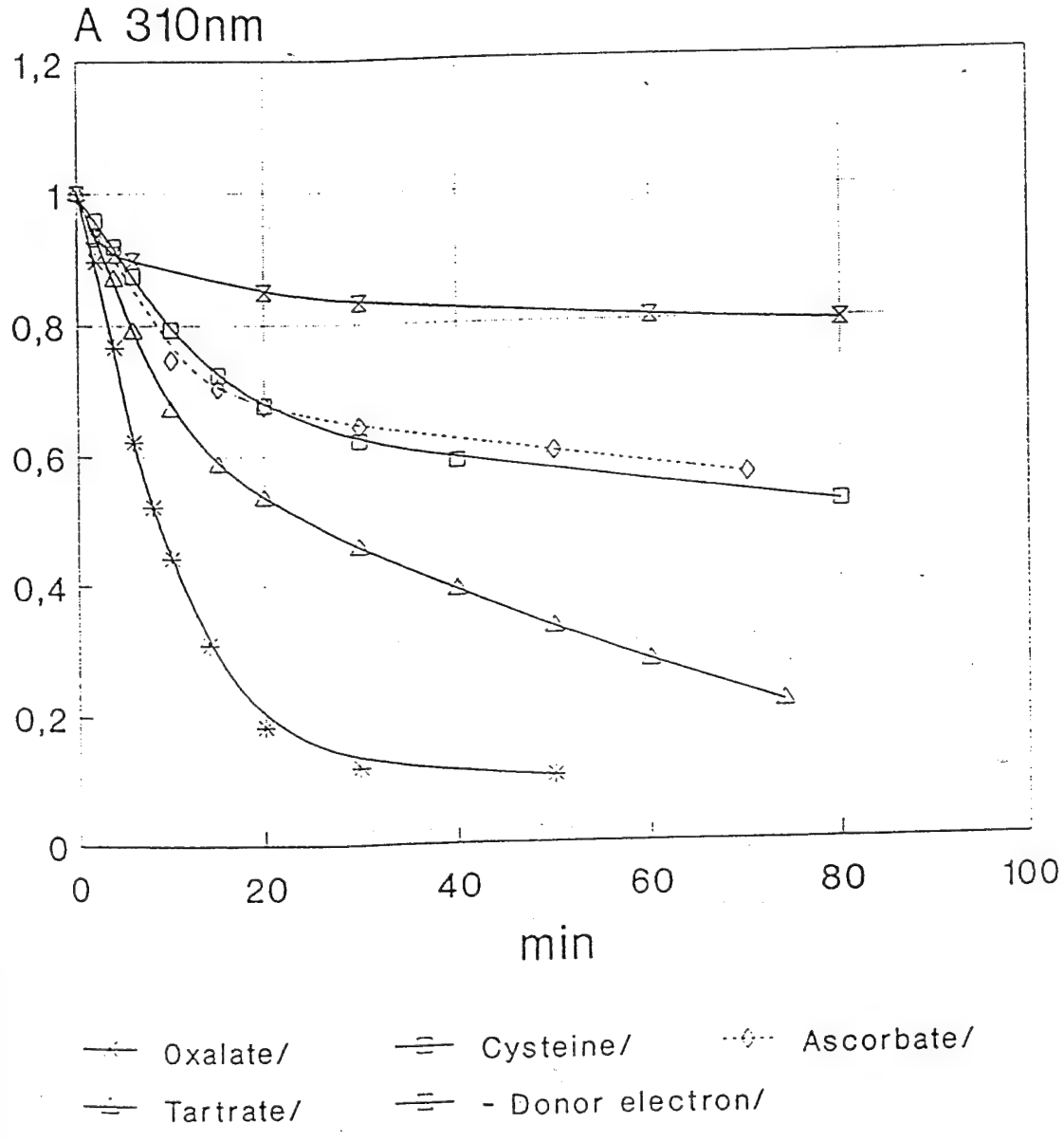

0.25mg/ml Ferritin, 20mM donor electron,
pH 5.5, 50 mM MES, Light>300nm

FIGURE 7

Photoreduction of Cytochrome by Ferritin

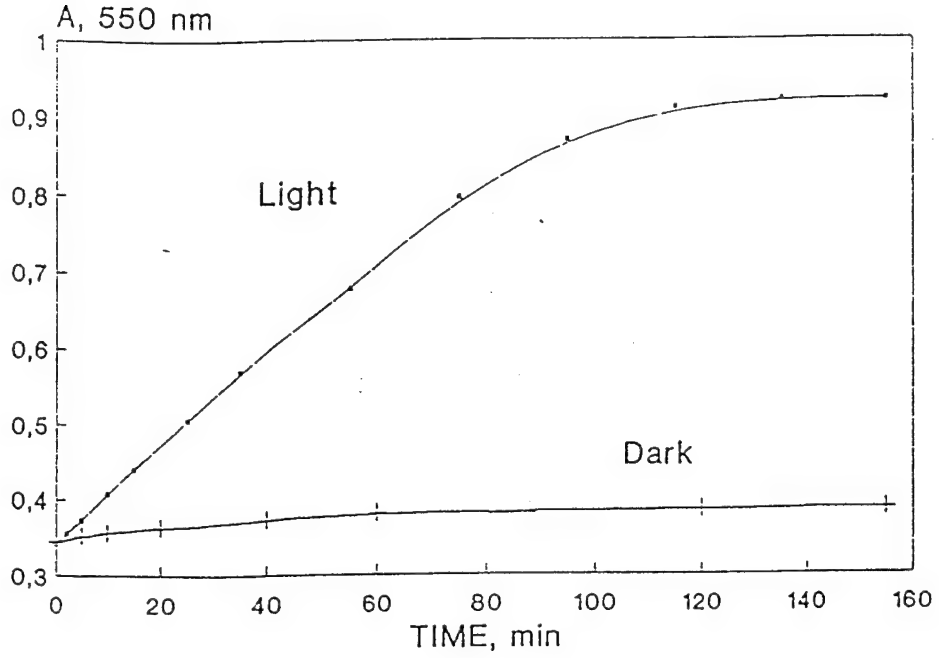

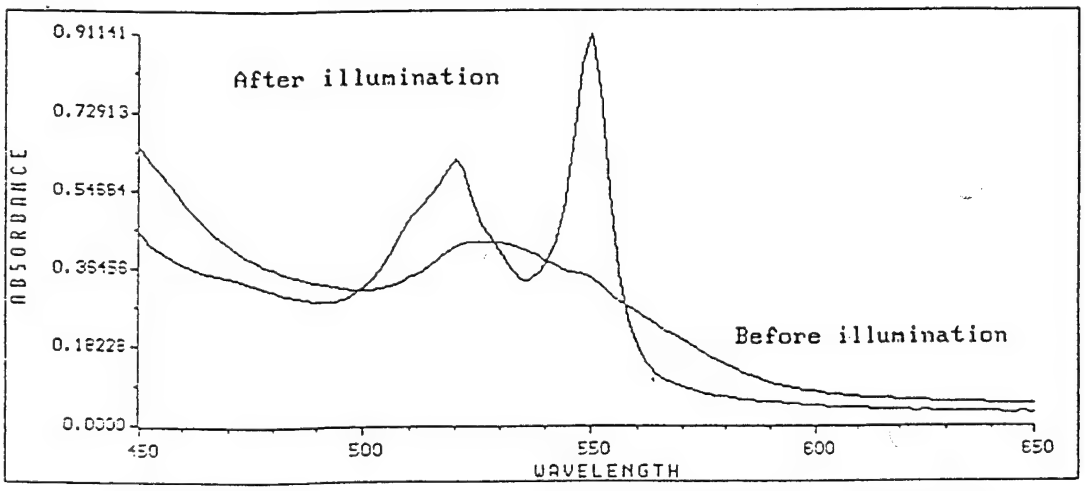

FIGURE 8

Photoreduction of DV by Ferritin

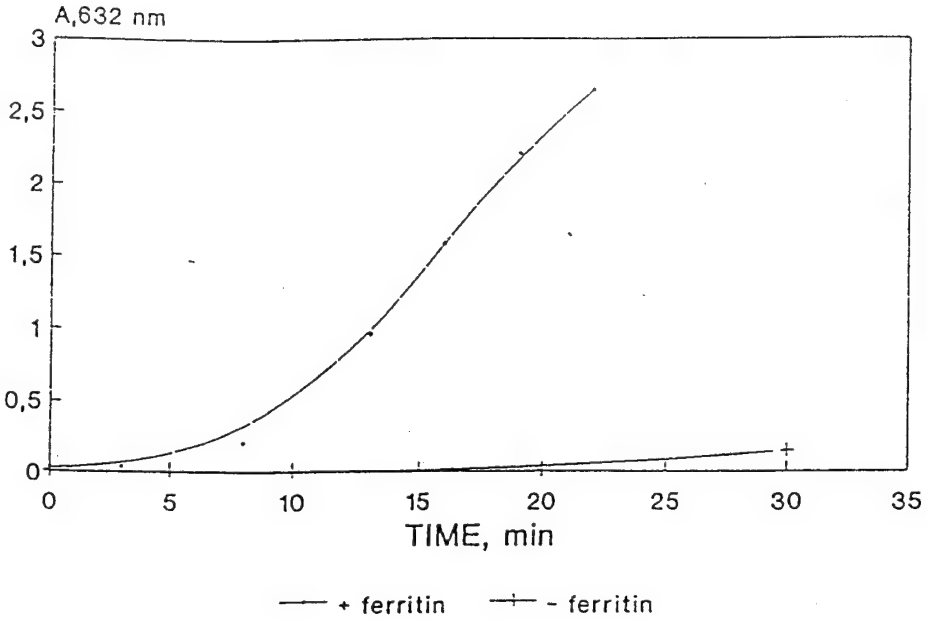

tartrate 0.1M, L>440nm, argon

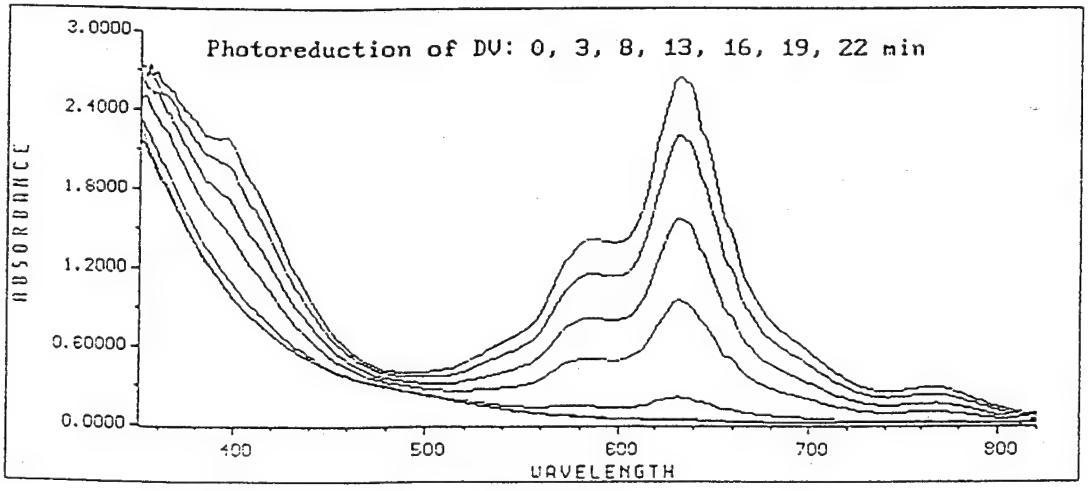

FIGURE 9

Photoreduction of Cytochrome by Ferritin as a Function of Light Intensity

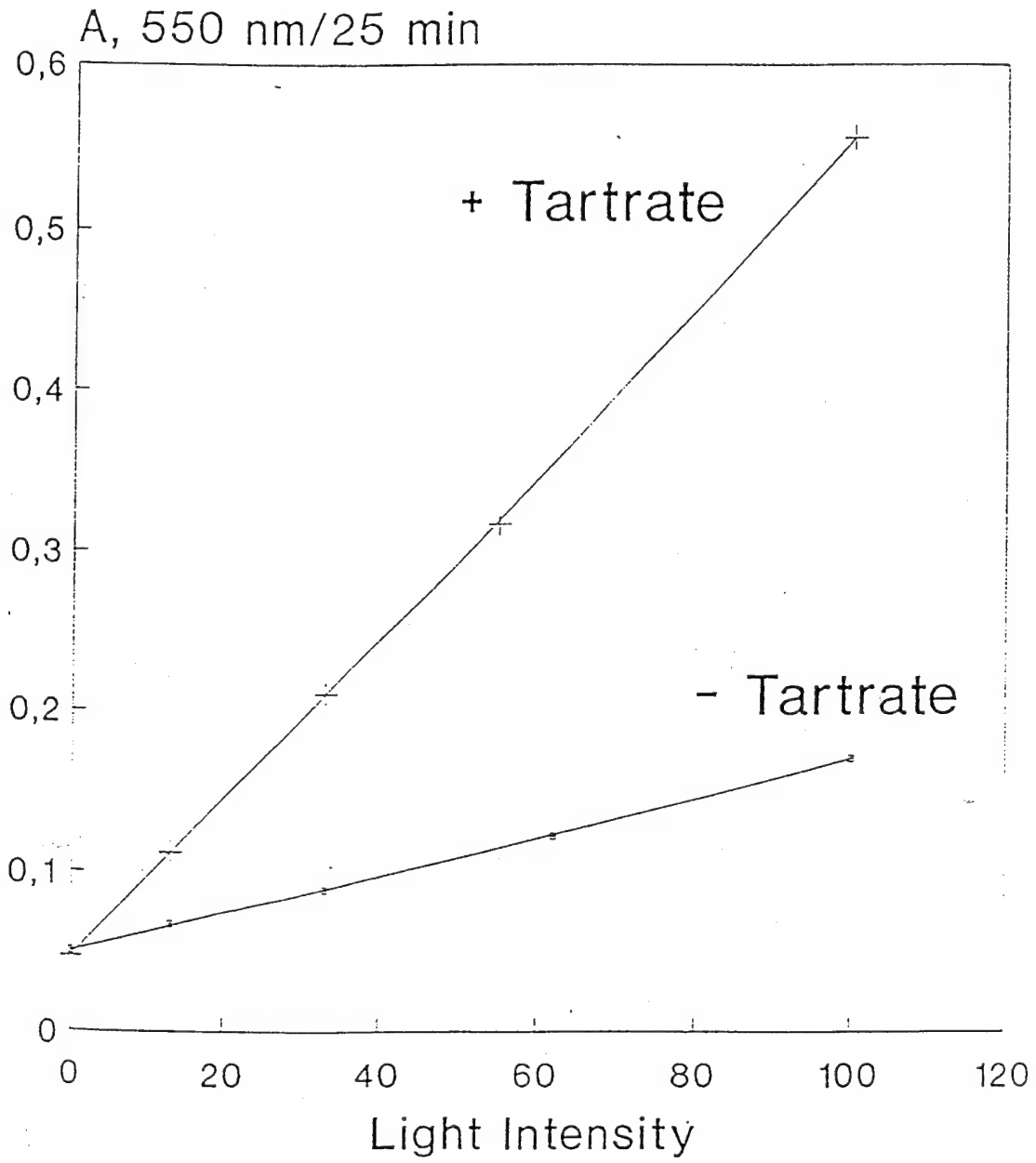

Cytochrome 32mkM. Ferritin 0.5 mg/ml
TES 0.05M, pH 7.0, Light>440nm
Tartrate 0.02M

FIGURE 10

Photoreduction of Cytochrome by Ferritin

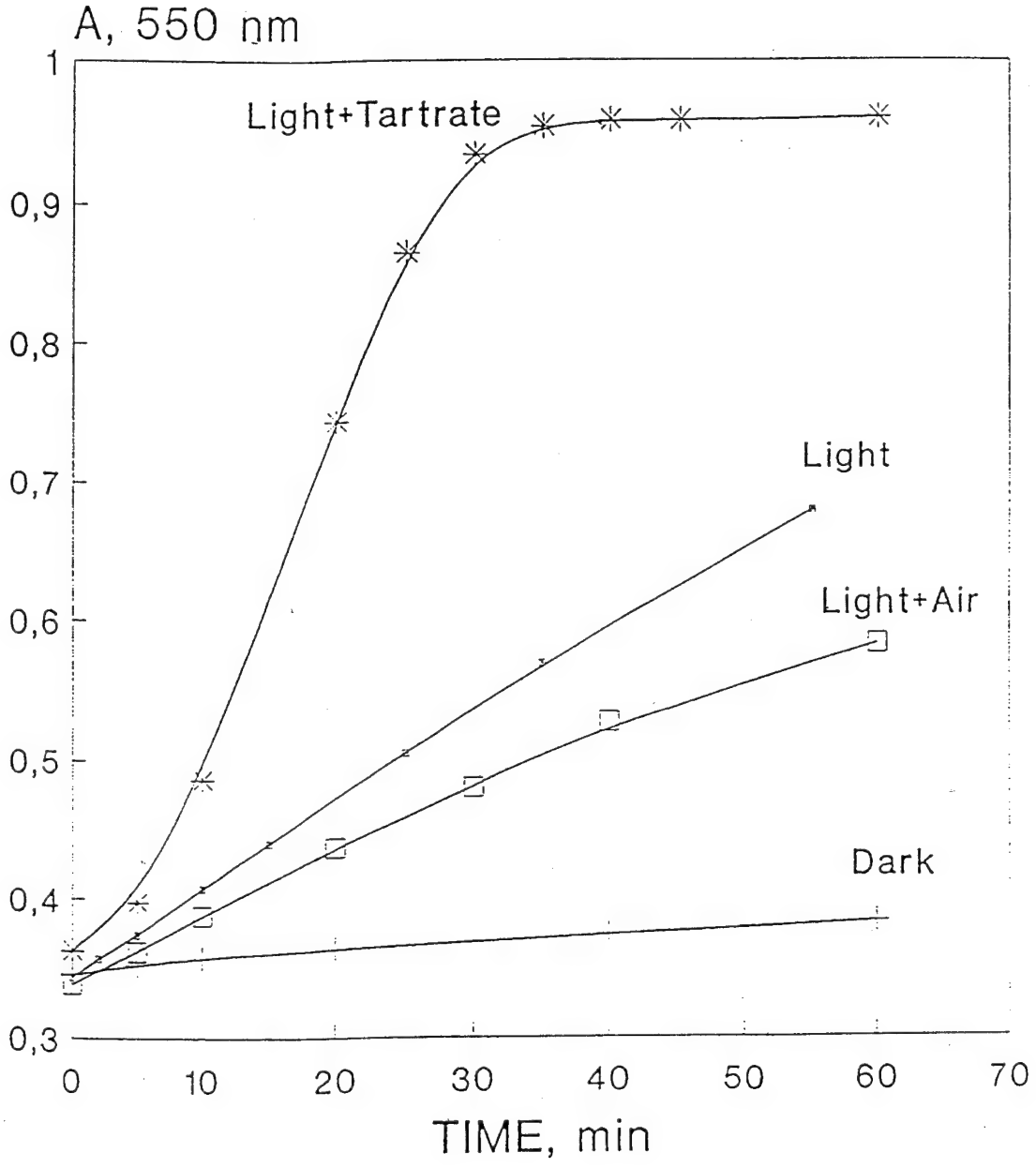

C 32mkM, F 1mkM; TES 0.05M, pH 7,0;
0.01M Tartrate, Light>440nm

FIGURE 11

LASER PHOTOLYSIS OF FERRITIN/PROPYLVIOLOGEN SULFONATE AQUEOUS SOLUTIONS

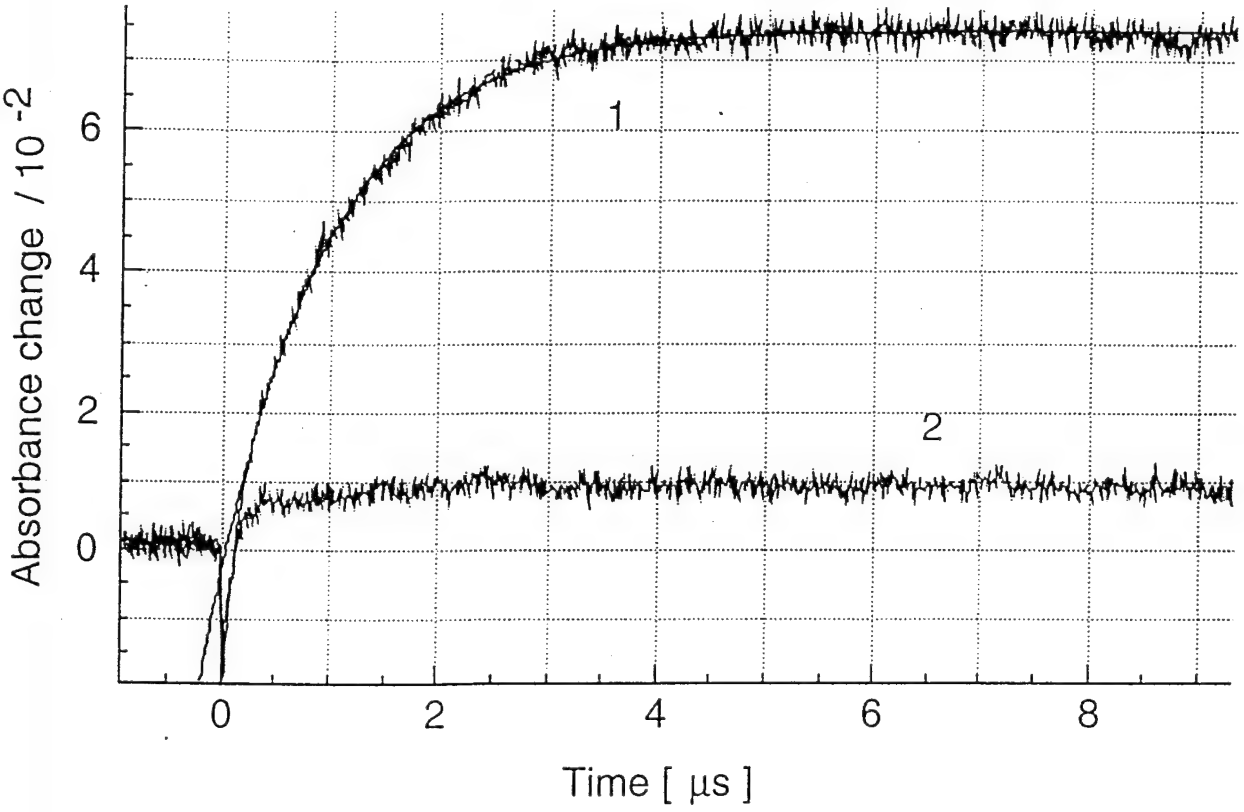

1) Ferritin (horse spleen) 0.11 mg/ml = 2. 10^{-7} M, Fe(III) in Ferritin = $1.64 \cdot 10^{-4}$ M,, PVS = 10^{-3} M, tartrate = 10^{-1} M, CAPS buffer pH =10, Ar bubbled, λ_{ext}= 347 nm, λ_{obs}= 602 nm.

2) blank, all conditions identical except no ferritin added

FIGURE 12

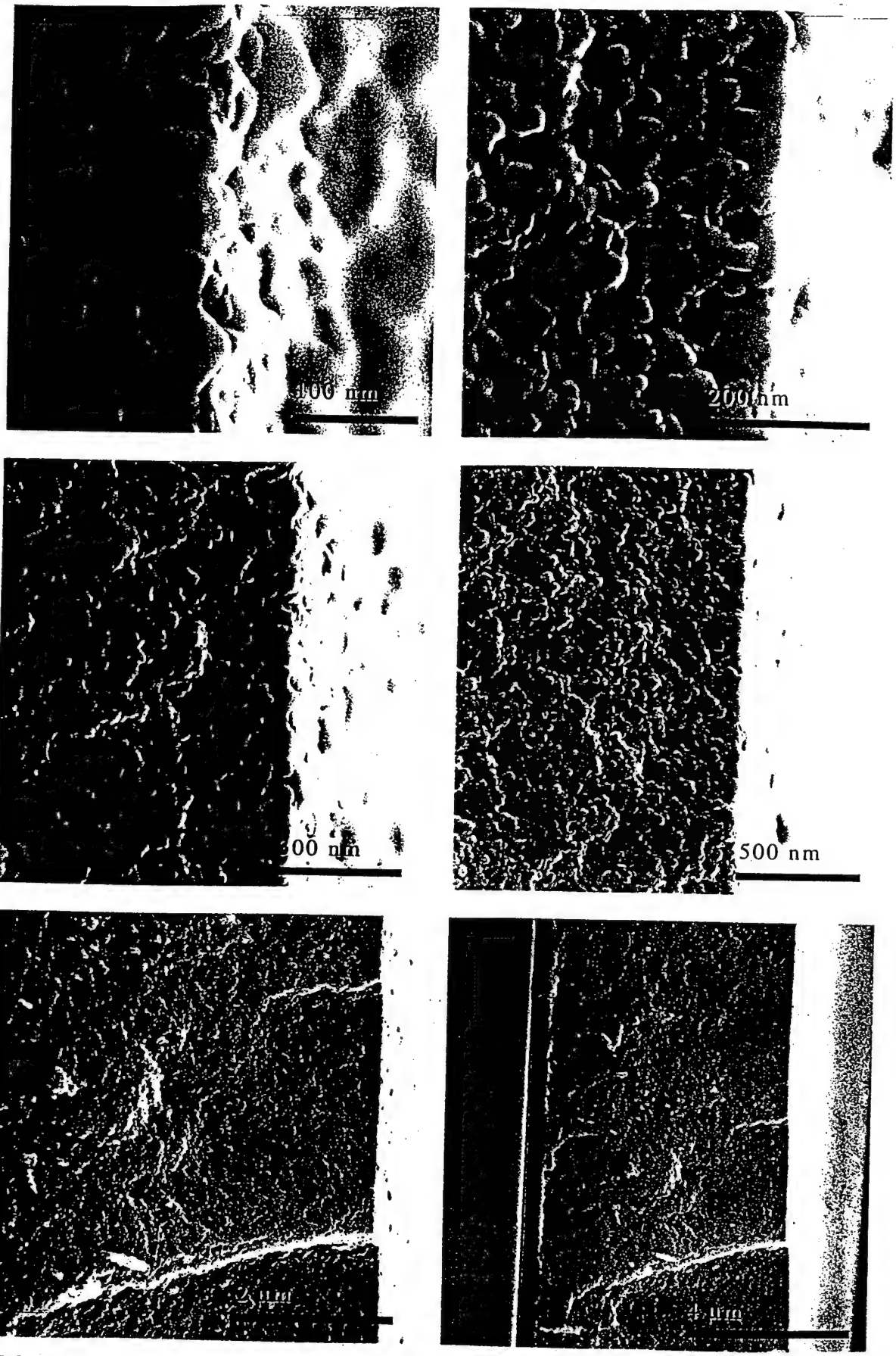

SCANNING ELECTRON MICROSCOPE IMAGES OF NANOCRYSTALLINE FILM EDGES IN WO_3, PREPARATION E12, WORKING ELECTRODE

WHITE LIGHT PHOTOCURRENT/VOLTAGE PLOT FOR WATER OXIDATION USING WO_3 (E12) WE

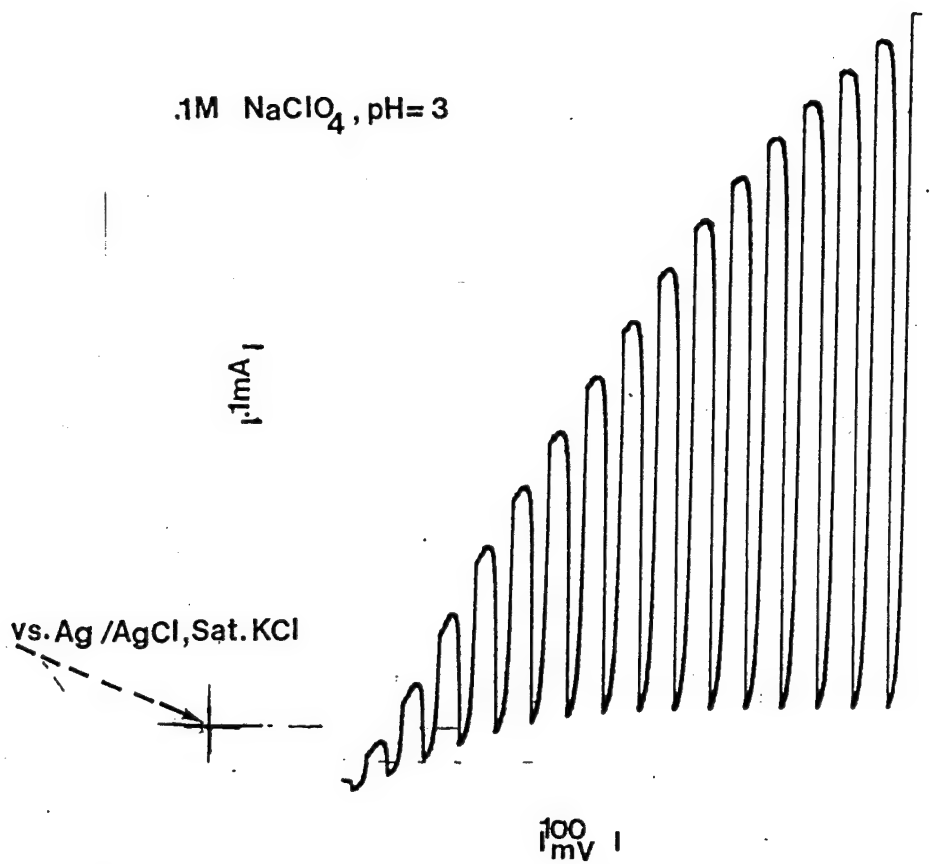

FIGURE 13

FIGURE 14

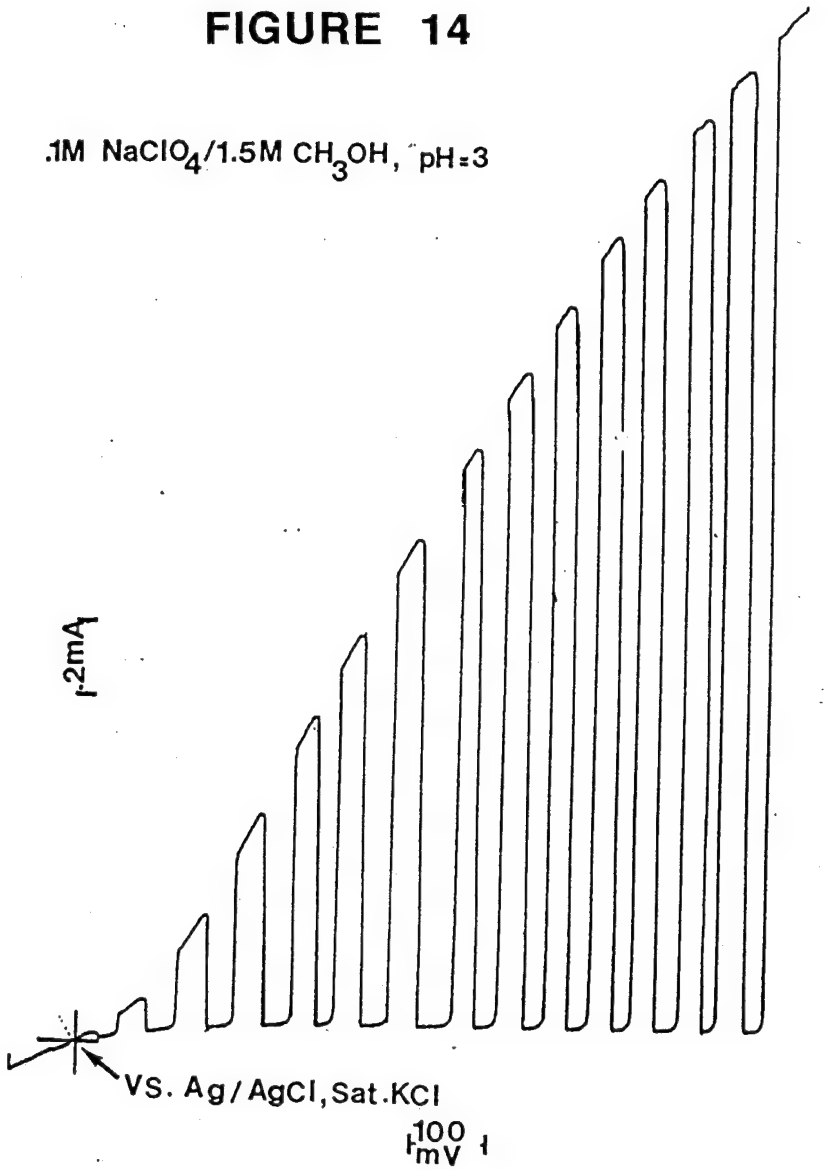

WHITE LIGHT PHOTOCURRENT/VOLTAGE PLOT FOR METHANOL OXIDATION USING WO_3 (E12) WE

wavel	dw	I(w)	I(w)xdw	∂I,100%	∑,100%	∑(I(w)xdw)	IPCE(%)	wave(nm)	wavel	∂I,100%	IPCE(%)extr	∂I,WO3	∑,WO3
305.000	5.000	0.009	0.046	1.131	1.131	0.046	0.490933	490	305.000	1.131	63.33	0.72	0.72
310.000	5.000	0.041	0.204	5.100	6.231	0.250	0.596867	480	310.000	5.100	67.96	3.47	4.18
315.000	5.000	0.104	0.520	13.197	19.428	0.770	1.152248	470	315.000	13.197	71.27	9.41	13.59
320.000	5.000	0.174	0.872	22.503	41.932	1.642	2.561227	460	320.000	22.503	74.59	16.78	30.37
325.000	5.000	0.238	1.190	31.176	73.108	2.831	5.109492	450	325.000	31.176	79.54	24.80	55.17
330.000	5.000	0.381	1.905	50.698	123.806	4.736	9.396237	440	330.000	50.698	84.49	42.84	98.01
335.000	5.000	0.376	1.880	50.790	174.596	6.616	15.865033	430	335.000	50.790	88.66	45.03	143.04
340.000	5.000	0.420	2.098	57.512	232.108	8.714	25.091255	420	340.000	57.512	92.82	53.38	196.42
345.000	5.000	0.423	2.115	58.845	290.953	10.829	36.536144	410	345.000	58.845	93.37	54.94	251.36
350.000	7.500	0.466	3.497	98.692	389.644	14.325	49.013467	400	350.000	98.692	93.92	92.69	344.05
360.000	10.000	0.501	5.014	145.568	535.212	19.339	61.833906	390	360.000	145.568	93.39	135.94	479.99
370.000	10.000	0.642	6.421	191.594	726.806	25.760	74.801710	380	370.000	191.594	85.69	164.18	644.17
380.000	10.000	0.667	6.667	210.440	937.247	32.427	85.691699	370	380.000	210.440	74.80	157.41	801.58
390.000	10.000	0.695	6.946	218.463	1155.710	39.573	93.385283	360	390.000	218.463	61.83	135.08	936.67
400.000	10.000	0.976	9.764	314.968	1470.677	49.337	93.918058	350	400.000	314.968	49.01	154.38	1,091.04
410.000	10.000	1.116	11.162	369.066	1839.744	60.499	92.819836	340	410.000	369.066	36.54	134.84	1,225.89
420.000	10.000	1.141	11.411	386.502	2226.245	71.910	84.494630	330	420.000	386.502	25.09	96.98	1,322.86
430.000	10.000	1.033	10.330	358.218	2584.463	82.240	74.585740	320	430.000	358.218	15.87	56.83	1,379.70
440.000	10.000	1.255	12.548	445.252	3029.715	94.788	67.962851	310	440.000	445.252	9.40	41.85	1,421.54
450.000	10.000	1.471	14.707	533.722	3563.436	109.495	58.701532	300	450.000	533.722	5.11	27.27	1,448.81
460.000	10.000	1.542	15.416	571.684	4135.320	124.911	54.630149	290	460.000	571.684	2.56	14.65	1,463.46
470.000	10.000	1.524	15.237	577.531	4712.852	140.148	0.000000	280	470.000	577.531	1.15	6.65	1,470.11
480.000	10.000	1.569	15.693	607.471	5320.323	155.841			480.000	607.471	0.60	3.64	1,473.75
490.000	10.000	1.483	14.834	586.182	5906.505	170.675			490.000	586.182	0.49	2.88	1,476.63
500.000	10.000	1.493	14.926	601.855	6508.360	185.601			500.000	601.855			

TABLE 1

ACTION SPECTRA FOR METHANOL OXIDATION ON WO_3 FILMS

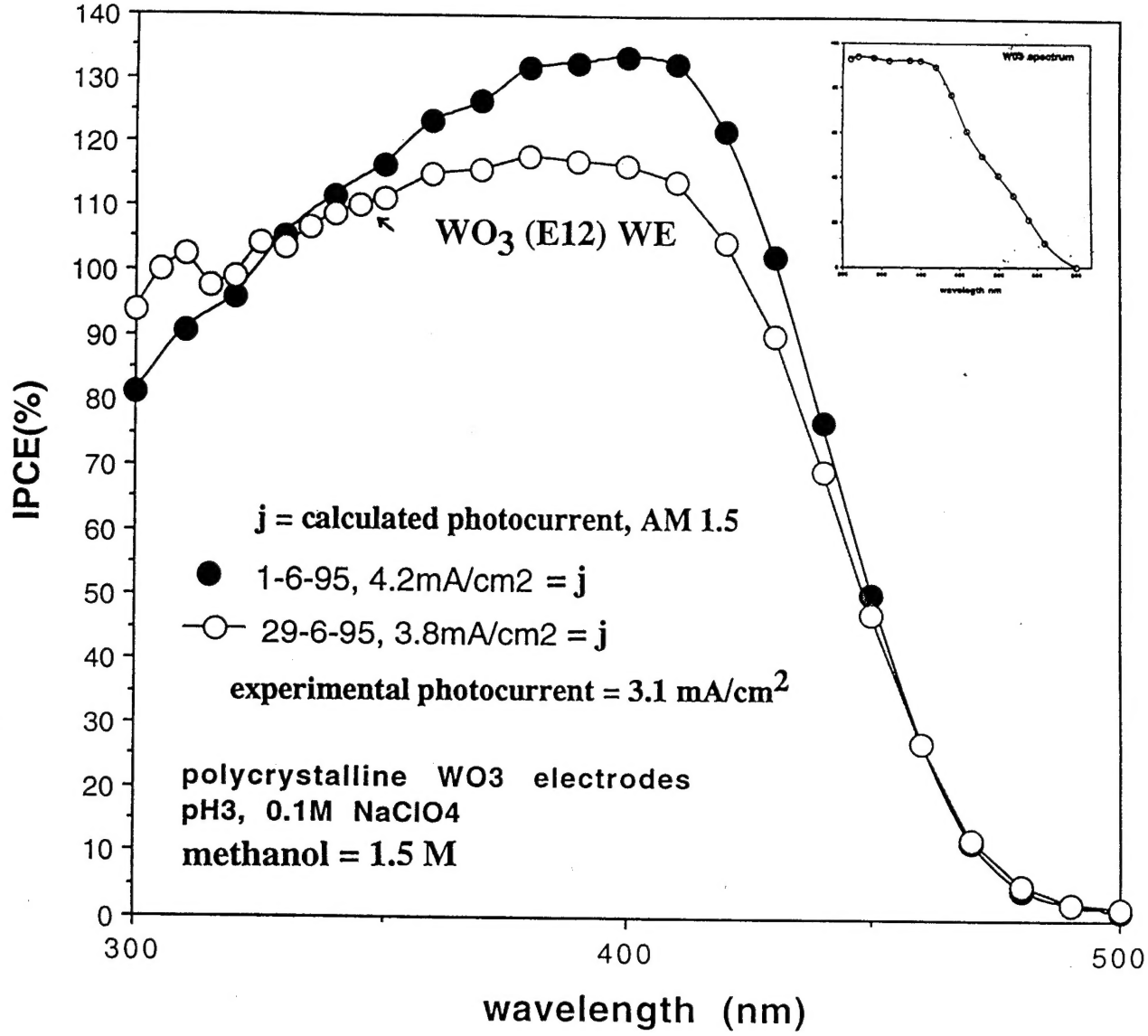

FIGURE 15

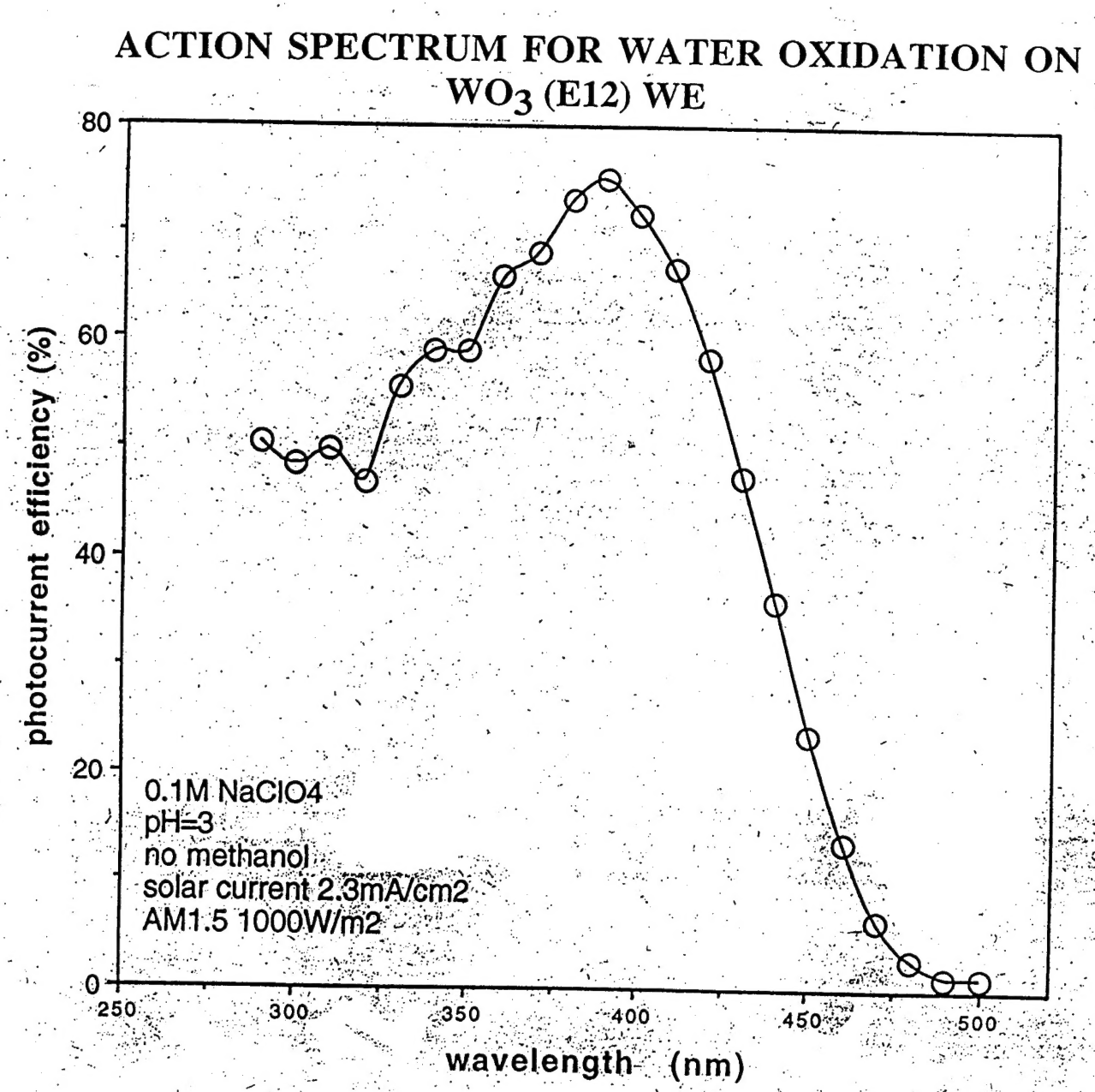
ACTION SPECTRUM FOR WATER OXIDATION ON
WO3 (E12) WE
photocurrent efficiency (%)
80
60
40
20
0
0.1M NaClO4
pH=3
no methanol
solar current 2.3mA/cm2
AM1.5 1000W/m2
250
300
350
400
450
500
wavelength (nm)

FIGURE 16

ACTION SPECTRUM FOR PHENOL OXIDATION ON TiO_2 FILMS

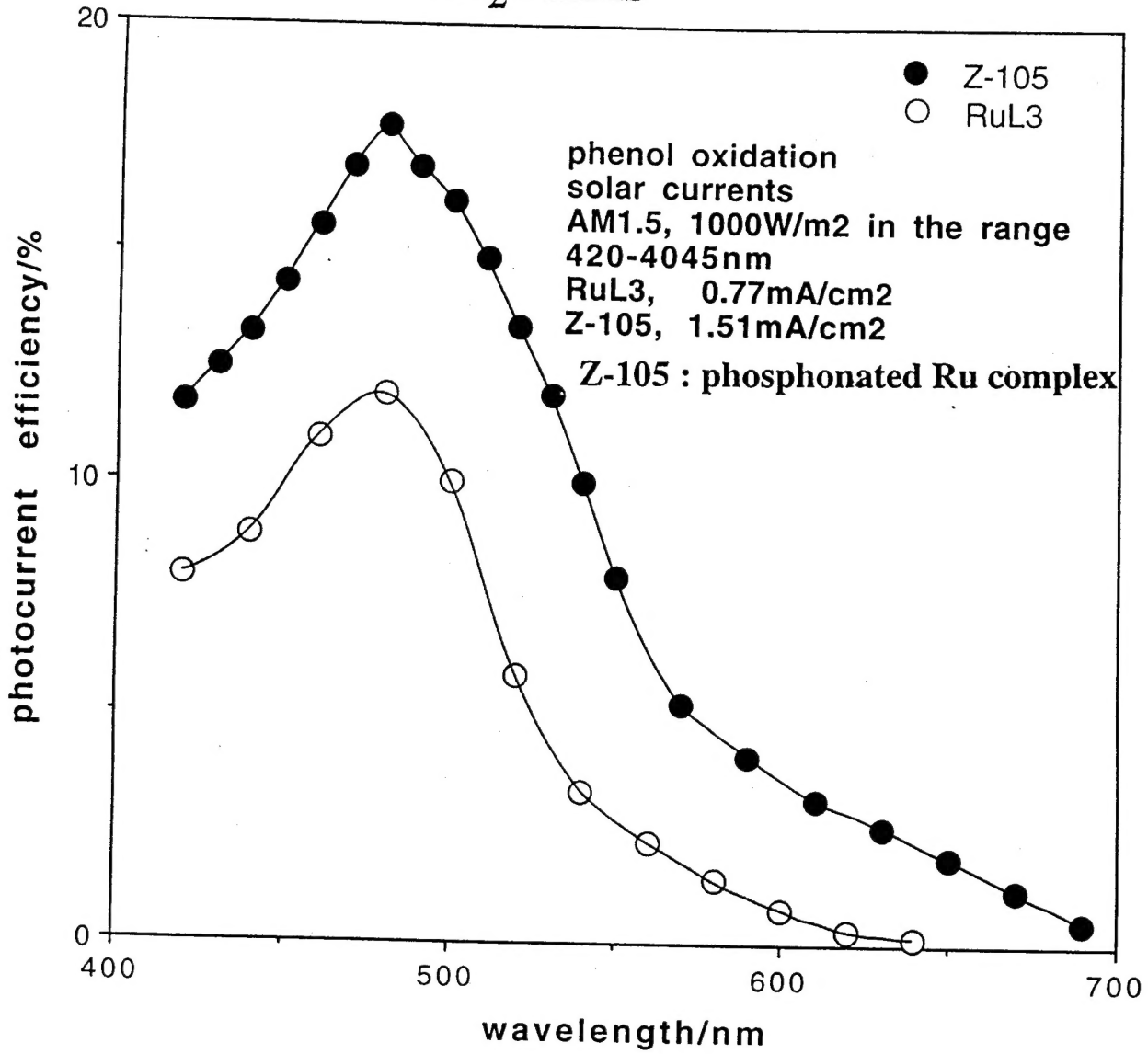

FIGURE 17